AIP | The Journal of Chemical Physics

Reaction dynamics of O(1D) + HCOOD/DCOOH investigated with time-resolved Fourier-transform infrared emission spectroscopy

Shang-Chen Huang, N. T. Nghia, Raghunath Putikam, Hue M. T. Nguyen, M. C. Lin, Soji Tsuchiya, and Yuan-Pern Lee

Citation: The Journal of Chemical Physics **141**, 154313 (2014); doi: 10.1063/1.4897418
View online: http://dx.doi.org/10.1063/1.4897418
View Table of Contents: http://scitation.aip.org/content/aip/journal/jcp/141/15?ver=pdfcov
Published by the AIP Publishing

Reaction dynamics of O(^{1}D) + HCOOD/DCOOH investigated with time-resolved Fourier-transform infrared emission spectroscopy

Shang-Chen Huang,[1] N. T. Nghia,[2] Raghunath Putikam,[1] Hue M. T. Nguyen,[3] M. C. Lin,[1,a)] Soji Tsuchiya,[1,a),b)] and Yuan-Pern Lee[1,4,a)]
[1]*Department of Applied Chemistry and Institute of Molecular Science, National Chiao Tung University, Hsinchu 30010, Taiwan*
[2]*School of Chemical Engineering - Hanoi University of Science and Technology, Hanoi, Vietnam*
[3]*Center for Computational Science and Faculty of Chemistry, Hanoi National University of Education, Hanoi, Vietnam*
[4]*Institute of Atomic and Molecular Sciences, Academia Sinica, Taipei 10617, Taiwan*

(Received 22 August 2014; accepted 26 September 2014; published online 21 October 2014)

We investigated the reaction dynamics of O(^{1}D) towards hydrogen atoms of two types in HCOOH. The reaction was initiated on irradiation of a flowing mixture of O_3 and HCOOD or DCOOH at 248 nm. The relative vibration-rotational populations of OH and OD ($1 \leqq v \leqq 4$, $J \leq 15$) states were determined from time-resolved IR emission recorded with a step-scan Fourier-transform spectrometer. In the reaction of O(^{1}D) + HCOOD, the rotational distribution of product OH is nearly Boltzmann, whereas that of OD is bimodal. The product ratio [OH]/[OD] is 0.16 ± 0.05. In the reaction of O(^{1}D) + DCOOH, the rotational distribution of product OH is bimodal, but the observed OD lines are too weak to provide reliable intensities. The three observed OH/OD channels agree with three major channels of production predicted with quantum-chemical calculations. In the case of O(^{1}D) + HCOOD, two intermediates HOC(O)OD and HC(O)OOD are produced in the initial C−H and O−D insertion, respectively. The former undergoes further decomposition of the newly formed OH or the original OD, whereas the latter produces OD via direct decomposition. Decomposition of HOC(O)OD produced OH and OD with similar vibrational excitation, indicating efficient intramolecular vibrational relaxation, IVR. Decomposition of HC(O)OOD produced OD with greater rotational excitation. The predicted [OH]/[OD] ratio is 0.20 for O(^{1}D) + HCOOD and 4.08 for O(^{1}D) + DCOOH; the former agrees satisfactorily with experiments. We also observed the v_3 emission from the product CO_2. This emission band is deconvoluted into two components corresponding to internal energies $E = 317$ and 96 kJ mol^{-1} of CO_2, predicted to be produced via direct dehydration of HOC(O)OH and secondary decomposition of HC(O)O that was produced via decomposition of HC(O)OOH, respectively. © *2014 AIP Publishing LLC*. [http://dx.doi.org/10.1063/1.4897418]

I. INTRODUCTION

The reactions of electronically excited oxygen atom O(^{1}D) with many atmospheric species have been extensive investigated because of their importance in atmospheric chemistry.[1,2] The reactions are typically characterized by an initial insertion of O(^{1}D) into the C−H bond of reactants to produce an energetic intermediate that proceeds via several reaction channels before further fragmentation.[3–6] In the case of O(^{1}D) + CH_4, the abstraction channel is also important according to the observation of OH product scattered in the forward and backward directions in significant proportions.[6]

Investigations of the reactions of O(^{1}D) with species that possess H atoms of two types is important because of the competition of two attacking sites for O(^{1}D) and also the competition of insertion or abstraction reactions. In particular, when a molecule, such as CH_3OH, possesses both C−H and O−H bonds, O(^{1}D) might insert into either bond; the former produces a new OH moiety that compete with the original OH moiety during further fragmentation. Previously, we reported the observations of rotationally resolved IR emission spectra of OH and OD that were produced from the reaction of O(^{1}D) with CH_3OD or CD_3OH.[7] For O(^{1}D) + CD_3OH, the product ratio [OH]/[OD] was 1.56 ± 0.36 with the rotational distribution of OD being nearly Boltzmann whereas that of OH being bimodal. For O(^{1}D) + CH_3OD, the product ratio [OH]/[OD] was 0.59 ± 0.14 and the rotational distribution of OH was nearly Boltzmann whereas that of OD was bimodal. With quantum-chemical calculations of the potential-energy surfaces (PES) and microcanonical rate coefficients of various channels, we concluded that the observed three internal distributions of OH are consistent with those produced via decomposition of the newly formed OH and the original OH moiety of $HOCH_2OH$ that is produced from insertion of O(^{1}D) into the C−H bond of CH_3OH, and decomposition of CH_3OOH that is produced via insertion of O(^{1}D) into the O−H bond of CH_3OH. The decomposition of the newly formed OH in $HOCH_2OH$ produces more vibrationally excited OH because of incomplete intramolecular vibrational

a)Authors to whom correspondence should be addressed. Electronic addresses: chemmcl@emory.edu, tsuchis@sepia.plala.or.jp, and yplee@mail.nctu.edu.tw.
b)Present address: Research Institute of Science and Engineering, Waseda University, Ookubo, Shinjuku-ku, Tokyo 169-8555, Japan.

relaxation (IVR), and decomposition of CH_3COOH produces OH with greater rotational excitation, likely due to a large torque angle during dissociation.

Although the observed [OH]/[OD] ratio in the reaction of $O(^1D) + CH_3OD$ (CD_3OH) indicated a preference for the formation of OD (OH) from the hydroxyl moiety over the methyl moiety of CH_3OH, it is not in conflict with a theoretical prediction that $O(^1D)$ prefers to attack the methyl moiety of CH_3OH. The reason is partly that, upon insertion of $O(^1D)$ into a C−H bond to form $HOCH_2OH$, the subsequent dissociation occurred for both the newly formed OH and the original OH group, and partly because some inserted intermediate $HOCH_2OH$ also decomposed to form $H + OCH_2OH$ and $H_2O + H_2CO$, whereas the decomposition of CH_3OOH, produced from insertion of $O(^1D)$ into the O−H bond, produced mainly $CH_3O + OH$.

We extended the investigation to the reaction of $O(^1D)$ with formic acid (HCOOH) in which the methyl moiety in CH_3OH is replaced by a formyl moiety. In addition to the fundamental importance of the reactivity towards H atoms of two types discussed previously, this reaction is related to the reaction of OH + HOCO that is important in combustion systems;[8] both reactions share a common intermediate HOC(O)OH and produce $CO_2 + H_2O$ or $CO_2 + H + OH$. Surprisingly, this reaction has been little studied; no report on the reaction kinetics or dynamics of this reaction is available. The only information is the infrared (IR) identification of the intermediate peroxyformic acid HC(O)OOH from the reaction of $O(^1D)$ with *trans*-HCOOH in a cryogenic matrix.[9]

Here we report our observations of rotationally resolved IR emission spectra of OH and OD that were produced from the reaction of $O(^1D)$ with HCOOD and DCOOH. In addition to the vibration-rotational distributions of OH and OD we determined also the ratio of [OH]/[OD]. We observed also unresolved emission of CO_2. To assist the interpretation of experimental data, we calculated quantum-chemically the PES of various reaction channels and predicted the branching ratios accordingly.

II. EXPERIMENTS

The step-scan Fourier-transform spectrometer (FTS) for emission detection was described previously;[10–12] only a brief summary is presented here. Ozone (O_3) and HCOOD or DCOOH were injected separately into the reaction chamber. A KrF laser (248 nm, 23 Hz) was employed to photolyze O_3 to form $O(^1D)$. A telescope mildly focused this photolysis beam to an area $\sim 12 \times 10$ mm^2 at the reaction center to yield a fluence ~ 55 mJ cm^{-2}. IR emission was collected with two Welsh mirrors (focal length 10 cm) before being detected with the InSb detector (rise time 0.34 μs and responsivity 3.2×10^6 V W^{-1}) of a step-scan FTS. The preamplified transient signal from the detector was further amplified 20 times with a voltage amplifier (bandwidth 1 MHz) before being digitized with an external data-acquisition board (12-bit, 25-ns resolution).

Data were typically averaged over 60 laser pulses at each scan step. For simultaneous detection of OH and OD, 4569 scan steps were performed to yield an interferogram resulting in spectra of resolution 0.8 cm^{-1} to cover a spectral range of 2170−3580 cm^{-1}. For detection of CO_2, 1883 scan steps were performed to yield an interferogram resulting in spectra of resolution 8 cm^{-1} to cover a spectral range of 1700–2400 cm^{-1}. To increase further the ratio of signal to noise, eight spectra recorded under similar conditions were averaged. The temporal response period of the detection system is approximately 1 μs, determined with an IR laser emission.[13] The spectral response function was calibrated with a black-body radiation source.

To decrease the collisional quenching of OH and OD, a minimal pressure yielding satisfactory signals was used: $P_{O3} = 12-16$ mTorr, P_{DCOOH} and $P_{HCOOD} \cong 84-88$ mTorr. Flow rates were $F_{O3} = 1.6-2.3$ sccm, F_{DCOOH} and $F_{HCOOD} = 12.7-12.8$ sccm, in which sccm denotes cm^3 min^{-1} under standard conditions (1 atm and 298.15 K). Approximately 60% of O_3 was dissociated upon irradiation at 248 nm according to the employed laser fluence, the reported absorption cross section of $\sim 1.1 \times 10^{-17}$ cm^2 molecule^{-1} for O_3, and a quantum yield of $\sim 0.90 \pm 0.05$ for the formation of $O(^1D)$ from O_3 at 248 nm.[14,15]

DCOOH (isotopic purity 98%) and HCOOD (isotopic purity 98%, both Cambridge Isotope Laboratories) were employed without further purification. For experiments with HCOOD, the reaction chamber was heated to 343 K under vacuum, followed by passivation with D_2O (10 Torr) at 298 K for 1 h. After evacuation, the system was filled with D_2O (10 Torr) overnight and was treated with passivation and evacuation three times before each experiment. Production and measurements of O_3 were described previously.[7] The formation of dimeric HCOOH has $\Delta G = -7.2$ kJ mol^{-1} at 343 K.[16] At 343 K and partial pressure 0.10 Torr, the fraction of dimer is estimated to be <0.2% of the monomeric HCOOH.

III. COMPUTATIONAL METHOD

The geometries of the reactants, transition states and products for the reaction $O(^1D)$ + HCOOH were optimized with hybrid density functional theory (DFT) at the B3LYP/6-311++G(3df,2p) level.[17] The stationary points were identified as local minima or transition states according to a vibrational analysis. The geometries of transition states were then used as an input for IRC calculations to verify the connectivity of the reactants and products. An energy path representing a barrierless insertion or an association process was obtained on calculating the potential-energy curve at the CASPT2(8,8)/6-311++G(3df,2p)//CAS(8,8)/6-311G++G(3df,2p) level of theory along its reaction coordinate: O···H (for C−H or O−H abstraction) from its equilibrium separation to ~8 Å at step size 0.2 Å and O···C (for C−H insertion) and O···O (for O−H, C−O, or C=O insertion) from its equilibrium separation to ~5 Å at step size 0.1 Å. For more accurate evaluation of energies, we calculated energies at single-points on the B3LYP-optimized geometries with the CCSD(T)/6-311++G(3df,2p) method.[18] The relative energies presented in the PES are corrected for unscaled zero-point vibrational energies (ZPVE). For the abstraction channels, of

which the transition states could not be found with the DFT method, we optimized the structures and calculated the energies with the MRCI(8,8)/6-311++G(3df,2p)//CAS(8,8)/6-311++G(3df,2p) method.[19] These calculations were performed using the MOLPRO program,[20] whereas all DFT-based calculations were performed with the Gaussian 09 package.[21]

Rate coefficients and product branching ratio in the temperature range 200−2000 K were calculated with the Master Equation (RRKM/ME) method implemented in the VARIFLEX code[22] based on the microcanonical RRKM (Rice-Ramsperger-Kassel-Macus) theory.[23,24] The numbers of states for the tight transition states were evaluated according to the rigid-rotor harmonic-oscillator approximation. For those paths involving hydrogen atom transfer, Eckart tunneling[25]corrections were made in calculations of the rate coefficients; however, the effect was found to be negligible, as one would expect, because of the large excess energies above those transition states involved; see Table SI in the supplementary material.[26] For the barrierless transition states, a Morse potential $V(R) = D_e\{1 - \exp[-\beta(R - R_e)]\}^2$ was used to represent the potential energy along the minimum energy path (MEP) of an individual reaction coordinate. In the above equation, D_e is the binding energy of a dissociation reaction excluding the contribution of the zero-point vibrational energy, R is the reaction coordinate, and R_e is the equilibrium value of R at the stable intermediate structure. In the RRKM calculations, the Lennard-Jones parameters for HOC(O)OH and HC(O)OOH were approximated with parameters $\sigma = 3.95$ Å and $\varepsilon/\kappa = 519$ K of HCOOH.[27–29]

IV. RESULTS AND DISCUSSION

A. IR emission of OH and OD from O(¹D) + DCOOH

Figure 1 shows the time-resolved spectra in the spectral region 3000−3600 cm^{-1} recorded at 1-μs intervals for the first 3 μs upon irradiation at 248 nm of a flowing mixture of O_3/DCOOH (12/88, 0.100 Torr, 343 K); O(¹D) was generated on photolysis of O_3 to react with DCOOH. Sharp lines located in these regions are identified as the $\Delta v = -1$ transitions of OH. Weak lines of OD in the region 2200−2600 cm^{-1} were also observed, but the intensities of OD lines were too small to provide reliable information. In addition to sharp lines of OH and OD, a broad feature that covered a region 1800–2400 cm^{-1} was observed. We assigned this feature to the emission of the antisymmetric stretching (ν_3) mode of vibrationally excited CO_2, to be discussed in Sec. IV C.

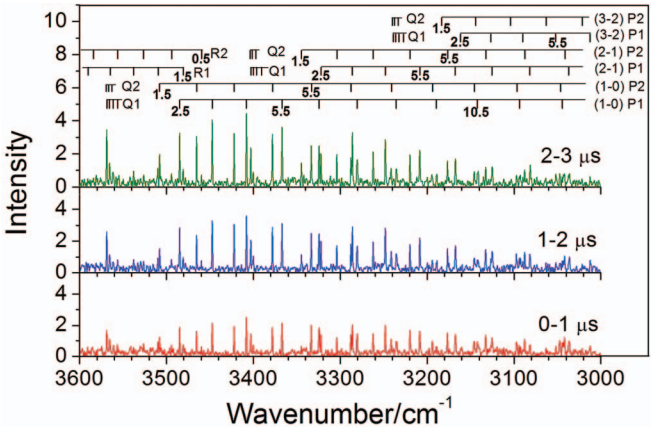

FIG. 1. Observed IR emission spectra of the reaction system O(¹D) + DCOOH recorded at 1-μs intervals. The spectral resolution is 0.8 cm^{-1}. Partial pressures of O_3 and DCOOH are 12 and 88 mTorr, respectively. The assignments of vibration-rotational transitions are shown as stick diagrams for OH; the numbers correspond to J' and (v'–v'') represents the vibrational transition.

For the assignment of our observed emission spectra, please refer to our previous paper.[7] Most Λ doublet *e* and *f* lines are unresolved because of insufficient resolution. For $J' > 10.5$, the *e*/*f* splitting exceeds 1 cm^{-1}, resulting in broadened or partially resolved lines. In this experiment, we made no attempt to separate the populations of the *e* and *f* transitions, but used the total population for each vibration-rotational transition. To analyze these observed lines, we assumed a Gaussian line shape and performed curve fitting on each line, including overlapped ones.

The intensities of emission lines of OH and OD rise toward their maxima ~4 μs after irradiation of the flowing sample at 248 nm. Because the initial concentration of DCOOH, ~2.4×10^{15} molecule cm^{-3}, was much greater than that of O_3, the condition of pseudo-first-order reaction is valid. The rate coefficient for the reaction O(¹D) + HCOOH is unreported. We expect the rate coefficient of the reaction to be slightly smaller than that of O(¹D) + CH_3OH, reported to be 5×10^{-10} cm^3 $molecule^{-1}$ s^{-1},[30] because of the smaller number of H atoms. The corresponding pseudo-first-order rate coefficient $k^I < 1.2 \times 10^6$ s^{-1} is in accord with the observed rise time for emission of OH.

The micropopulation of OH was determined from spectral lines integrated at 1-μs intervals after irradiation. Each vibration-rotational line in the P branch was normalized with the instrument spectral-response function and divided by its Einstein *A* coefficient[31] to yield a relative population $P(v', J', F')$. In Fig. 2, the logarithm of the micropopulation defined as $P(v', J', F')/(2J' + 1)$, is plotted as a function of the rotational energy that is defined as the average of the *e* and *f* term values from which the vibrational term value is subtracted. The micropopulations of the F_1 and F_2 components are similar. The rotational distribution of OH ($v' = 1$ and $v' = 2$) is evidently not singly exponential; we thus fitted it with biexponential functions and derived rotational temperatures T_R for the low-*J* and the high-*J* components, respectively. For 0−1 μs, T_R are 1470 ± 70 and 540 ± 40 K for the high-*J* and low-*J* components of $v' = 1$, respectively, and 820 ± 60 and 430 ± 30 K for the high-*J* and low-*J* components of $v' = 2$, respectively. For $v' = 3$, because of the limited levels observed, we fitted them with only a single exponential function with $T_R = 250 \pm 60$ K. The bimodal rotational distribution suggests formation of OH from at least two reaction channels.

To derive the nascent rotational temperatures, we estimated the quenching effects on measuring the rotational temperature as a function of time, as shown in Fig. S1 of the supplementary material.[26] The correction factors for the average energy in the 0−1 μs range to the nascent one are

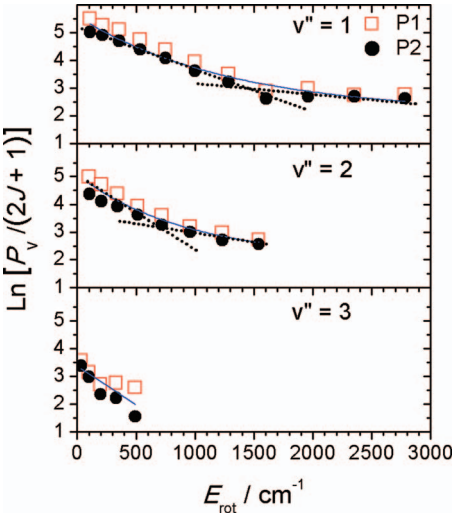

FIG. 2. Semilogarithmic plots of the rotational populations of OH as a function of the rotational energy E_{rot} in respective vibrational states formed from the O(^{1}D) + DCOOH reaction. The average period is 0−1 μs. Solid lines represent the fitting; dashed lines represent a bimodal fitting.

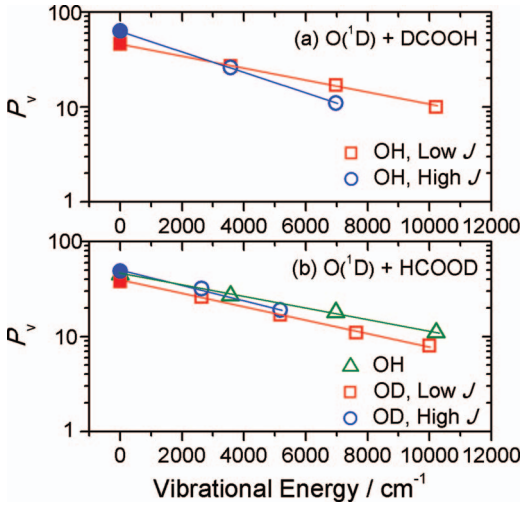

FIG. 3. Relative vibrational populations of OH and OD produced from (a) O(^{1}D) + DCOOH and (b) O(^{1}D) + HCOOD as a function of vibrational energy. Populations in $v = 0$ are derived by extrapolation. The data for OD from O(^{1}D) + DCOOH were unobtainable because of a poor signal-to-noise ratio.

approximately 1.03 ± 0.14 for the high-J component and 1.06 ± 0.15 for the low-J component, indicating that rotational quenching plays an insignificant role during the first 1 μs.

We obtained relative vibrational populations ($v' = 1$):($v' = 2$):($v' = 3$) = 1.00:0.63:0.36 for the low-J component and ($v' = 1$):($v' = 2$) = 1.00:0.43 for the high-J component. We assumed a Boltzmann distribution of vibrational population and estimated the population of level $v' = 0$ to be 1.76 ± 0.10 times that of $v' = 1$ for the low-J component on extrapolation from the populations of levels $v' > 1$. Similarly, the population of $v' = 0$ was estimated to be 2.43 ± 0.30 times that of $v' = 1$ for the high-J component. After renormalization, we derived relative vibrational populations ($v' = 0$):($v' = 1$):($v' = 2$):($v' = 3$) = 46:27:17:10 for the low-J component of OH and ($v' = 0$):($v' = 1$):($v' = 2$) = 63:26:11 for the high-J component of OH. As the correction for vibrational quenching is small, these values are taken as nascent vibrational energies, as shown in Fig. 3(a). With an assumption of a Boltzmann distribution, the vibrational temperatures are 9700 ± 300 and 5800 ± 300 K, respectively, for the low-J and high-J components of OH. Using this distribution of vibrational populations, we calculated the average vibrational energies E_v of OH to be 38 ± 4 and 20 ± 3 kJ mol^{-1} for the low-J and high-J components, respectively, as listed in Table I; these values should be taken as the lower limits of the vibrational energy because emission bands from higher vibrational levels might have some contributions but were too weak to observe.

The average rotational energies E_r of OH are calculated to be 7 ± 2 and 25 ± 4 kJ mol^{-1}, respectively, for the low-J and high-J components of OH. After correction for the rotational quenching according to the factors discussed above, the nascent rotational energies are 7 ± 2 and 26 ± 4 kJ mol^{-1} for the low-J and high-J components of OH, respectively, as listed in Table I.

TABLE I. Summary of experimental results for reactions O(^{1}D) + HCOOD/DCOOH.

	O(^{1}D) + DCOOH[a]		O(^{1}D) + HCOOD		
	OH			OD	
	low-J	high-J	OH	low-J	high-J
T_R ($v' = 1$)[b]/K	580 ± 60	1530 ± 150	490 ± 60	450 ± 60	1180 ± 160
T_R ($v' = 2$)[b]/K	450 ± 30	830 ± 40	400 ± 60	380 ± 80	850 ± 110
T_R ($v' = 3$)[b]/K	250 ± 60		270 ± 30	350 ± 40	
T_R ($v' = 4$)[b]/K				350 ± 50	
E_R[b]/kJ mol^{-1}	7 ± 2	26 ± 4	8 ± 2	6 ± 2	25 ± 6
T_v/K	9700 ± 300	5800 ± 300	10 600 ± 400	9100 ± 300	7900 ± 500
E_v[c]/kJ mol^{-1}	38 ± 4	20 ± 3	40 ± 4	38 ± 4	22 ± 3
[OH]/[OD][c]				0.16 ± 0.05	

[a]Unable to determine OD because of small intensity.
[b]Nascent values, extrapolated from data at 0−5 μs to $t = 0$.
[c]Including estimated population at $v = 0$; see text.

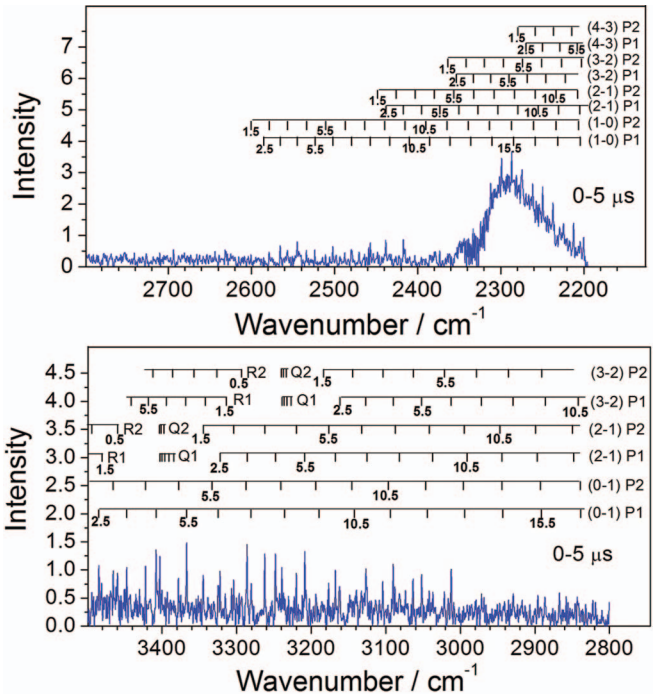

FIG. 4. Observed IR emission spectra of the reaction system O(^{1}D) + HCOOD integrated for 1–5 μs. The spectral resolution is 0.8 cm^{-1}. Partial pressures of O_3 and HCOOD are 12 and 88 mTorr, respectively. The assignment of vibration-rotation transitions are given as stick diagrams; the number corresponds to J' and (v'–v'') represents the vibrational transition.

B. IR emission of OH and OD from O(^{1}D) + HCOOD

To understand the relative reactivity of the insertion of O(^{1}D) into the C−H and O−H bonds of HCOOH, we investigate also the reaction of O(^{1}D) + HCOOD; a flowing mixture of O_3/HCOOD (12/88, 0.100 Torr, 343 K) was irradiated at 248 nm. The time-resolved IR emission spectra observed after photolysis are shown in Fig. 4; because observed lines are weak, we integrated the spectra for the period 0−5 μs to achieve a satisfactory ratio of signal to noise. Similar to the reaction of O(^{1}D) + DCOOH, two groups of sharp lines located in regions 2800–3600 and 2200–2600 cm^{-1} are assigned as the $\Delta v = -1$ vibration-rotational transitions of OH and OD, respectively. In addition, a broad emission feature, assigned to the ν_3 emission band of vibrationally excited CO_2, is observed in the region 1800–2400 cm^{-1}, to be discussed in Sec. IV C.

The relative rotational micropopulations of the respective vibrational states of OH and OD are shown as a function of rotational energy in Fig. 5. The rotational distributions of OH are nearly singly exponential, whereas those of OD are biexponential, similar to those of OH produced in the reaction of O(^{1}D) + DCOOH. Following the method similar to that described in Sec. IV A, we derived, for OH in the range 0–5 μs, T_R = 430 ± 60, 430 ± 30, and 270 ± 30 K for $v' = 1-3$, respectively. For OD in the range 0−5 μs, T_R = 1100 ± 160, and 400 ± 50 K for the high-J and low-J components of v' = 1, respectively, and T_R = 750 ± 80 and 370 ± 40 K for the high-J and low-J components of $v' = 2$, respectively. For $v' = 3$ and 4, we fit them with a single exponential function with T_R = 340 ± 30 and 320 ± 50 K, respectively, because of the limited levels observed. The average rotational energies of

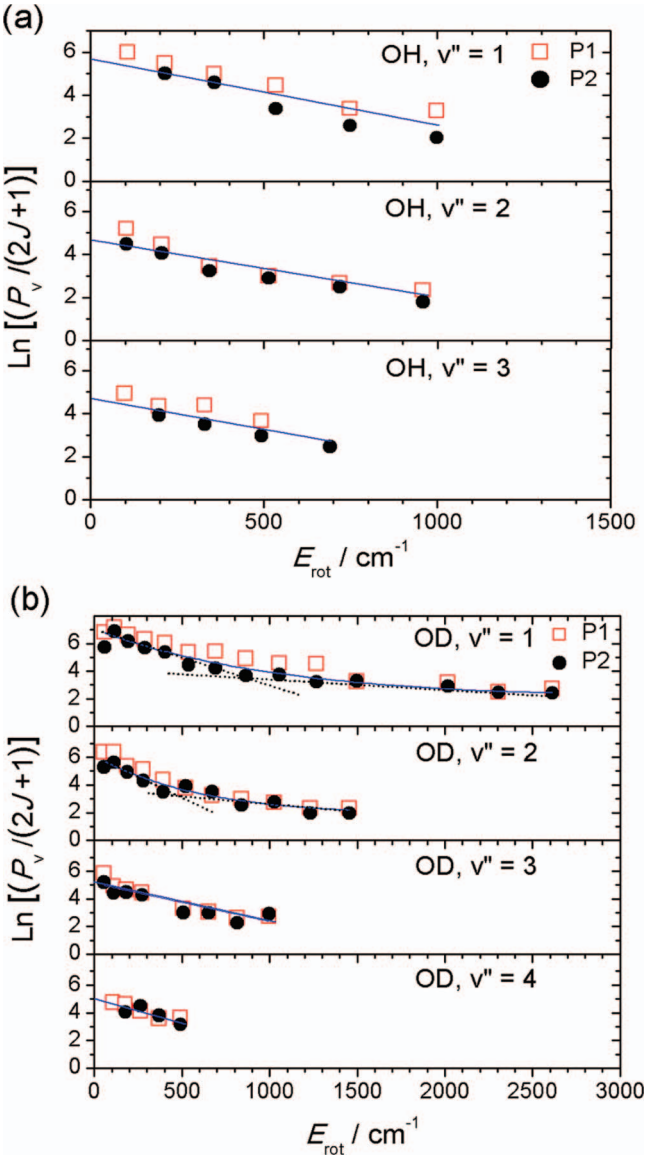

FIG. 5. Semilogarithmic plots of the rotational populations of (a) OH and (b) OD as a function of rotational energy E_{rot} in respective vibrational levels formed from the O(^{1}D) + DCOOH reaction. The average period is 0−5 μs. Solid lines represent the fitting; dashed lines represent a bimodal fitting.

OH and low-J and high-J components of OD observed in the period 0−5 μs are thus calculated to be 7 ± 2, 5 ± 2, and 22 ± 4 kJ mol^{-1}, respectively. Using data of OH from O(^{1}D) + DCOOH, the correction factors for the average energy in the 0−5 μs range to the nascent ones are approximately 1.10 ± 0.26 for the high-J component and 1.08 ± 0.29 for the low-J component. We hence derive the nascent rotational energy to be 8 ± 2 kJ mol^{-1} for OH, 6 ± 2 and 25 ± 6 kJ mol^{-1} for the low-J and high-J components of OD, respectively, as listed in Table I.

Similarly, the relative vibrational populations ($v' = 1$):($v' = 2$):($v' = 3$) = 1.00:0.66:0.38 for OH, ($v' = 1$):($v' = 2$):($v' = 3$):($v' = 4$) = 1.00:0.68:0.40:0.33 for the low-J component and ($v' = 1$):($v' = 2$) = 1.00:0.64 for the high-J component of OD were derived. Assuming a Boltzmann distribution of vibrational populations, we estimated the population of level $v' = 0$ to be 1.49 ± 0.21 and 1.59 ± 0.20 times that

of level $v' = 1$ for the low-J and high-J components of OD on extrapolation from the populations of levels $v' > 1$. The population of level $v' = 0$ was estimated to be 1.72 ± 0.17 times that of level $v' = 1$ for OH. After renormalization, we derived relative vibrational populations $(v' = 0):(v' = 1):(v' = 2):(v' = 3) = 45:27:18:11$ for OH, $(v' = 0):(v' = 1):(v' = 2):(v' = 3):(v' = 4) = 38:26:17:11:8$ and $(v' = 0):(v' = 1):(v' = 2) = 49:32:19$ for the low-J and high-J components of OD, respectively, as shown in Fig. 3(b). With an assumption of a Boltzmann distribution, the vibrational temperatures are $10\,600 \pm 400$ K for OH and 9100 ± 300 and 7900 ± 500 K for the low-J and high-J components of OH, respectively. Using this distribution of vibrational populations, we calculated the average vibrational energies to be 40 ± 4 kJ mol^{-1} for OH and 38 ± 4 and 22 ± 3 kJ mol^{-1} for the low-J and high-J components of OD, respectively, as listed in Table I; these values should be taken as the lower limits.

The ratio of total populations of OH ($v' = 1-3$) to those of OD ($v' = 1-4$) from O(^{1}D) + HCOOD are derived to be $(14 \pm 3)/(86 \pm 5)$, with the low-J component to the high-J component of OD $\sim$ 22/78. If we take into account the estimated populations of the $v' = 0$ levels of OH and OD, the ratio of total populations of OH ($v' = 0-3$) to those of OD($v' = 0-4$) becomes $(14 \pm 3)/(86 \pm 5) = 0.16 \pm 0.05$, with the low-$J$ component to the high-J component of OD $\sim$25/75. This ratio is much smaller than the value $(37 \pm 9)/(63 \pm 9) = 0.59 \pm 0.14$ reported for the reaction of O(^{1}D)+CH_3OD,[7] but if we consider the number of C−H bonds to be three in CH_3OD and one in HCOOD, the ratios observed in both reactions are consistent.

C. Emission spectra of CO_2 from O(^{1}D) + HCOOH

By comparison with the CO_2 emission spectra observed in the reaction O(^{1}D) + CO_2 (Ref. 32) we assigned the observed broad feature in the range 1800−2400 cm^{-1} as the ν_3 emission of highly internally excited CO_2. An emission spectrum of CO_2 recorded from 0 to 5 μs after irradiation of the O_3/HCOOH mixture at 248 nm is also shown in Fig. 6; this feature shows a maximum near 2280 cm^{-1} with a long tail extending toward 1800 cm^{-1}. At a later time, the long tail disappeared completely and the remaining feature agreed satisfactorily with the P and R branches of CO_2, with the band center located near 2327 cm^{-1} corresponding to the band origin of the transition $(v_3 = 1) \rightarrow (v_3 = 0)$ of CO_2 at 300 K.

We simulated the observed feature with an approximate method that we employed previously for analysis of the ν_3 emission of highly vibrationally excited CO_2 produced from O(^{1}D) + CO_2.[32] We introduced a polyad quantum number $v_b = 2v_1 + v_2$ with degeneracy g_b to describe the vibrational levels of CO_2 as (v_b, v_3); v_1 and v_2 are quantum numbers of strongly Fermi-coupled vibrational modes ν_1 and ν_2, respectively. The emission intensity of the transition $(v_b, v_3) \rightarrow (v_b, v_3 - 1)$, I $[(v_b, v_3) \rightarrow (v_b, v_3 - 1)]$, is proportional to $\omega[(v_b, v_3) \rightarrow (v_b, v_3 - 1)]$ $N(v_b, v_3)$ $A[(v_b, v_3) \rightarrow (v_b, v_3 - 1)]$, in which ω is the transition frequency for $(v_b, v_3) \rightarrow (v_b, v_3 - 1)$, $N(v_b, v_3)$ is the population of the (v_b, v_3) state, and A is the Einstein coefficient that is assumed to be proportional to v_3 but independent of v_b. To estimate the population distribution $N(v_b, v_3)$ in the (v_b, v_3) vibrational state, we assumed that an energy E^* is partitioned statistically into the rotation and vibrational degrees of freedom of CO_2 and the relative translational degree of freedom of CO_2 with its counter products, as described previously.[32]

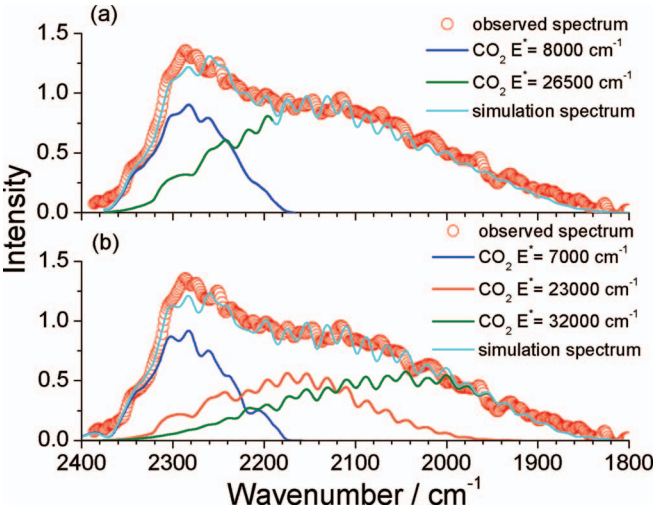

FIG. 6. Comparison of emission of CO_2 observed in the reaction O(^{1}D) + HCOOD (symbols o) with those deconvoluted with two components with $E^* = 8000$ and 26 500 cm^{-1} and a population ratio 53:47 (a); the contribution of each component is also shown. The simulated vibrational distributions based on statistical distribution of internal energies as discussed in the text are shown in (b).

The observed feature was approximately decomposed into two components with the statistically partitioned energy $E^* = 8000$ cm^{-1} = 96 kJ mol^{-1} and $E^* = 26\,500$ cm^{-1} = 317 kJ mol^{-1}, respectively, as shown in Fig. 6(a), with a population ratio $\sim$53:47. The population distributions of these two components are shown in Fig. 6(b).

D. Potential-energy surfaces and reaction mechanism

Formic acid possesses two stable geometric conformers in the gas phase—*cis* and *trans*. The ground state minimum has a planar *trans*-conformation with the two hydrogen atoms *trans* to the C−O bond.[33] The *trans*-conformer is predicted to be $\sim$17 kJ mol^{-1} more stable than the *cis*-structure, in agreement with the experimental value of 16 kJ mol^{-1}.[34] In this calculation, we considered only the reaction of *trans*-HCOOH with O(^{1}D).

After an exhaustive search, we established a potential-energy surface with 11 product channels PR1−PR11 in which the major paths led to products PR6 (CO_2 + H_2O), PR7 [OH + HC(O)O], and PR8 (OH + HOCO); the minor paths led to PR4 (H_2 + CO_3), PR5 (CO + H_2O_2), and other products. The major product channels are depicted in Fig. 7; a detailed PES including other minor channels is available in Fig. S2 of the supplementary material.[26] The optimized geometries of key intermediates and transition states are presented in Figs. 8 and 9, respectively; the geometries of other related species are shown in Fig. S3 of the supplementary material.[26] The transition states are denoted as Tx/y or TxPz in which x and y designate the intermediates (ISx and ISy) and Pz

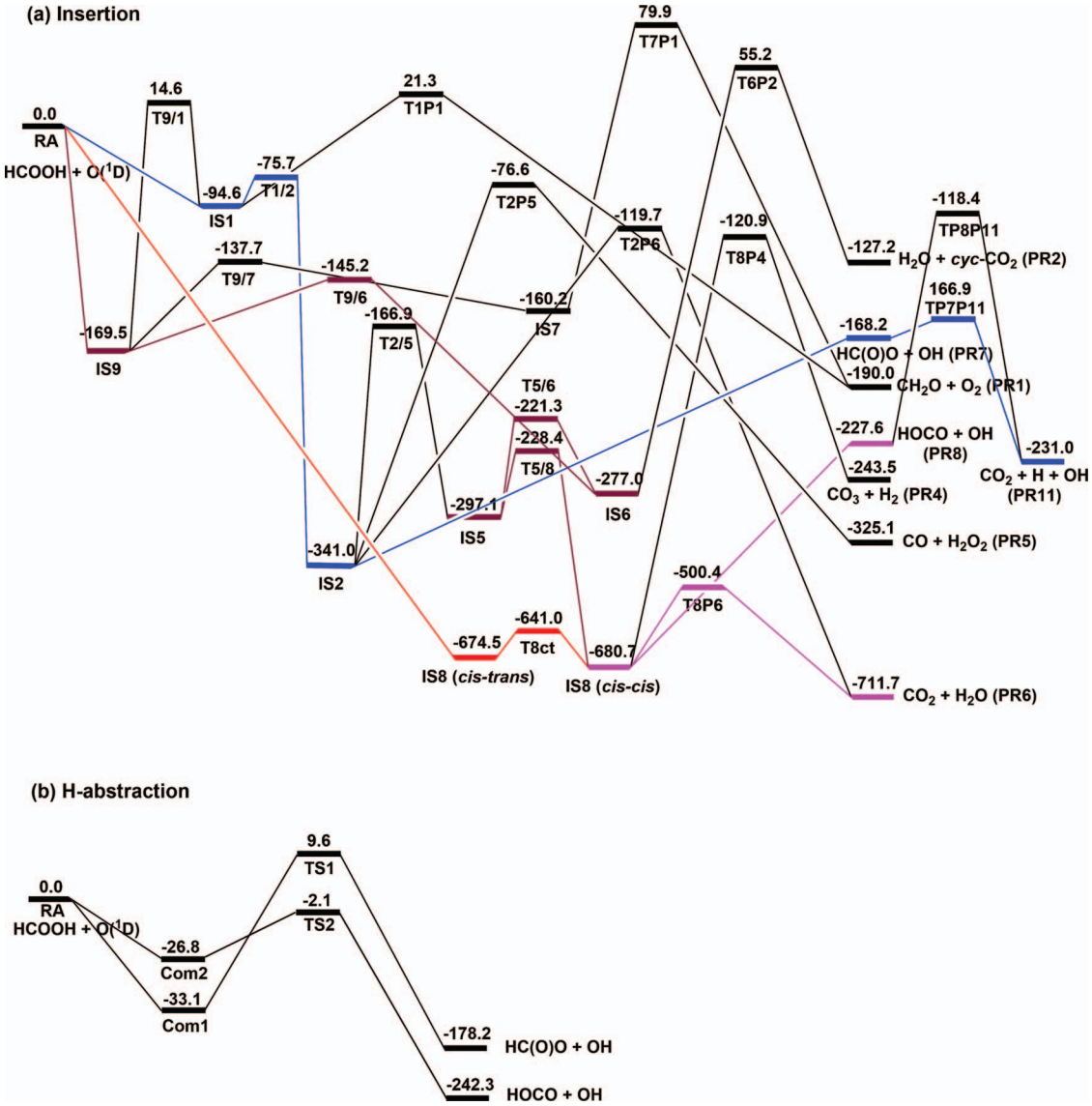

FIG. 7. Simplified potential-energy scheme of the reaction $O(^1D)$ + HCOOH. (a) Insertion reactions computed with the CCSD(T)/6-311++G(3df,2p)//B3LYP/6-311++G(3df,2p) + ZPVE method. (b) H-abstraction reactions computed with the MRCI(8,8)//CASSCF(8,8)/6-311++G(3df,2p) method. Energy is in kJ mol^{-1}.

designates the product (PRz) with which the transition state is associated.

The direct insertion into the C−H bond of HCOOH occurs without an intrinsic transition state to form a stable intermediate IS8, *cis-cis*-HOC(O)OH, with energy of −680.7 kJ mol^{-1} relative to the reactants; this energy is confirmed with the VTST MEP scan and is also in agreement with previous related work indicating that the $O(^1D)$ atom can insert directly into a C−H bond with large exothermicity.[7,35,36] Theoretical and experimental investigations[37–39] showed that IS8 has three structures of which the *cis-cis* is the most stable; the barrier for interconversion from *cis-trans* (∼6 kJ mol^{-1} greater in energy than *cis-cis*) to *cis-cis* conformers is only ∼33 kJ mol^{-1}. The *trans-trans* conformer has energy ∼38 kJ mol^{-1} above that of the *cis-cis* conformer. IS8 (*cis-cis*) and IS8 (*cis-trans*) can thus be regarded as one intermediate. Additional insertion reactions occur via two complexes in which $O(^1D)$ attacks the O atom in the OH group to form complex IS1, HC(O)O(O)H, and the O atom in the C=O group to form complex IS9, OOC(H)OH, with energies of −94.6 and −169.5 kJ mol^{-1}, respectively, relative to the reactants. Atoms in these complexes can migrate to form other intermediates or complexes; the energy-rich intermediates can undergo dissociation to yield products. For example, in IS1 the H atom in the OH group can migrate to the added O atom via T1/2 (−75.7 kJ mol^{-1}) to form IS2 (HC(O)OOH, −341.0 kJ mol^{-1}), or to the carbonyl O atom via T9/1 (14.6 kJ mol^{-1}) to form IS9, or to the C atom via T1P1 (21.3 kJ mol^{-1}), followed by C−O bond rupture to yield PR1 ($H_2CO + O_2$, −190.0 kJ mol^{-1}).

1. Formation of dehydration products PR6 ($CO_2 + H_2O$)

Several paths lead to PR6. $O(^1D)$ can insert directly into the C−H bond of HCOOH to form IS8, *cis-cis*-HOC(O)OH,

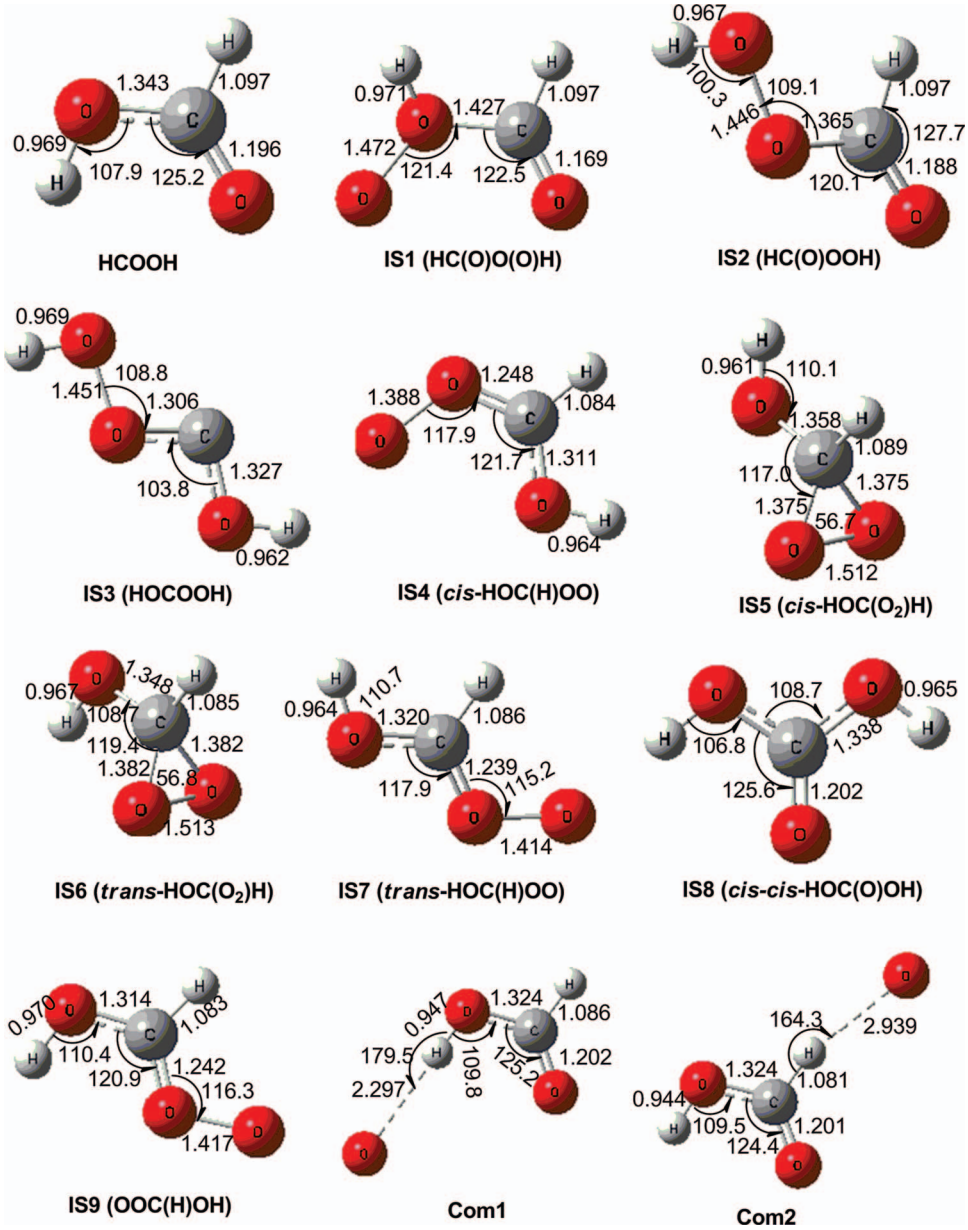

FIG. 8. Geometries of representative reactants and intermediates of the $O(^1D)$ + HCOOH reaction optimized with the B3LYP/6-311++G(3df,2p) method. Bond length in Å and bond angle in degree.

with a large exothermicity (−680.7 kJ mol^{-1}), followed by dehydration via T8P6 (−500.4 kJ mol^{-1}) to produce PR6 (CO_2 + H_2O; −711.7 kJ mol^{-1}). This process is clearly the most feasible because the first step to form IS8 is barrierless and highly exothermic, and the second step IS8 → PR6 proceeds via the transition state T8P6 with the lowest barrier. In addition, PR6 can also be produced on $O(^1D)$ attacking the C=O group of HCOOH without a barrier to give IS9, which then transforms to a triangular ring intermediate IS6 (*trans*-$HOC(O_2)H$; −277.0 kJ mol^{-1}) via T9/6 (−145.2 kJ mol^{-1}). IS6 subsequently transforms to IS5 (*cis*-$HOC(O_2)H$; −297.1 kJ mol^{-1}) via state T5/6 (−221.3 kJ mol^{-1}), and IS8 via T5/8 (−228.4 kJ mol^{-1}). The third path involving decomposition of IS2 to PR6 via T2P6 (−119.7 kJ mol^{-1}) is less important because it proceeds via a transition state with much greater energy. In summary, two main paths yielding PR6 are: RA → IS8 → PR6 and RA → IS9 → IS6 → IS5 → IS8 → PR6; when $O(^1D)$ reacts with HCOOD or DCOOH, PR6 becomes CO_2 + HDO.

2. Formation of radical products PR7 (OH + HC(O)O) and PR8 (OH and HOCO)

PR8 (OH + HOCO, −227.6 kJ mol^{-1}) are produced via several paths. First, IS8 dissociates directly to PR8 without a barrier. The product HOCO has two conformers, *cis* and *trans*; *cis*-HOCO can readily isomerize to *trans*-HOCO that lies ∼7.9 kJ mol^{-1} below *cis*-HOCO,[40] so the process IS8 → *cis*-HOCO + OH → *trans*-HOCO + OH can be regarded as entailing one step. Although the energy of PR8 is much greater than T8P6 (−500.4 kJ mol^{-1}), the formation of PR8 is competitive with formation of PR6 because IS8 → PR8 is

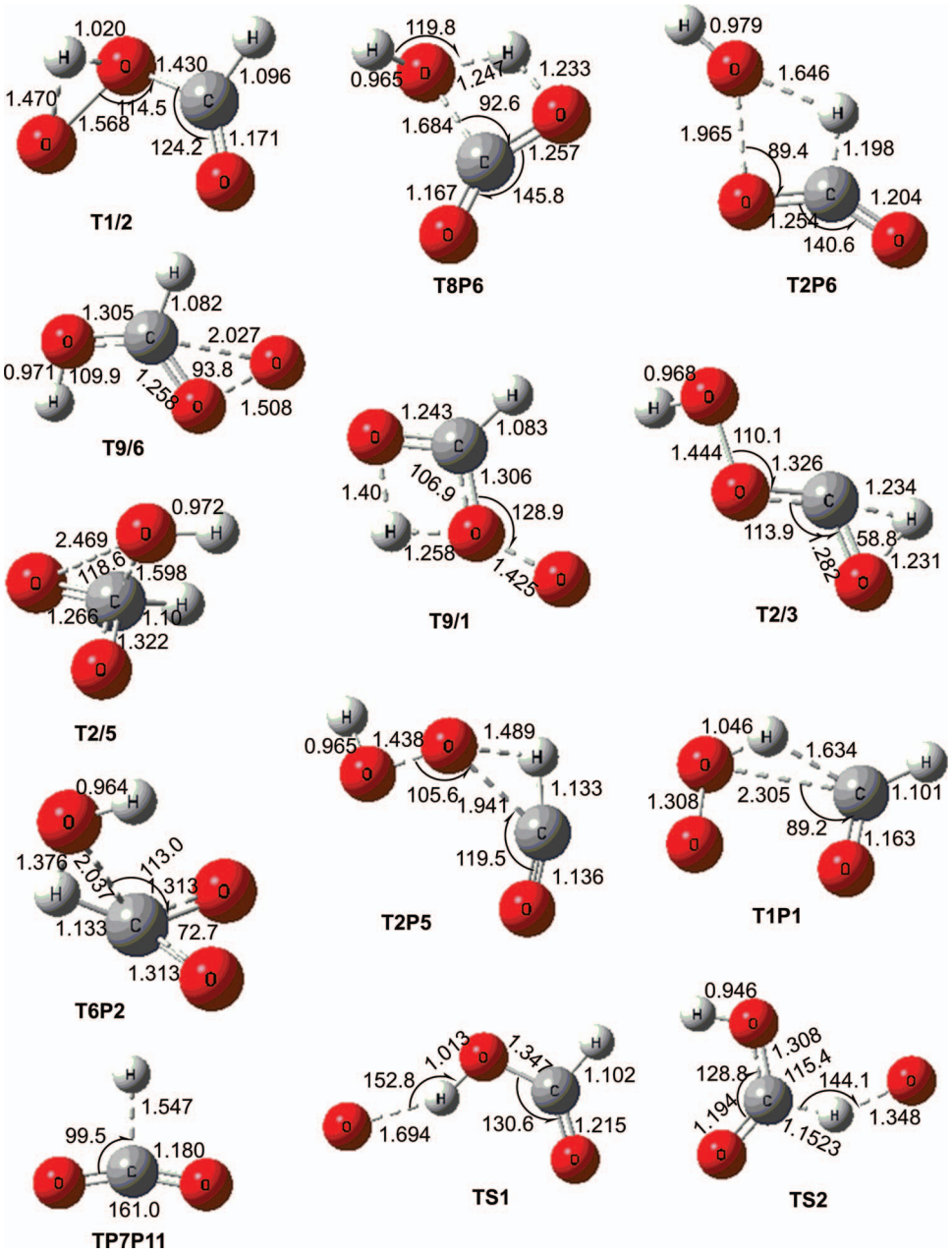

FIG. 9. Geometries of the representative transition states of the O(^{1}D) + HCOOH reaction optimized with the B3LYP/6-311++G(3df,2p) method. Bond length in Å and bond angle in degree.

barrierless. Other paths, such as IS1 → T1P8 (10.0 kJ mol^{-1}) → PR8 (Fig. S2 in the supplementary material),[26] are uncompetitive because of greater barriers. The two major paths for the formation of PR8 (OH + HOCO) are thus RA → IS8 → PR8 and RA → IS9 → IS6 → IS5 → IS8 → PR8. The two H atoms in IS8 play the same role; when RA involves HCOOD or DCOOH, PR8 hence represents both products OH + DOCO and OD + HOCO.

PR7 (OH + HC(O)O, −168.2 kJ mol^{-1}) is produced mainly from IS1 (−94.6 kJ mol^{-1}), which readily isomerizes to form IS2 (−341.0 kJ mol^{-1}) via T1/2 (−75.7 kJ mol^{-1}); the O−O bond in IS2 ruptures to yield PR7. IS2 can also isomerize to form IS3 or IS5 via T2/3 (−23.0 kJ mol^{-1}) or T2/5 (−166.9 kJ mol^{-1}), respectively, or dissociate to yield other products: PR4 (CO_3 + H_2), PR5 (CO + H_2O_2), and PR6 (CO_2 + H_2O) via T2P4, T2P5, and T2P6 with relative energies of −28.5, −76.6, and −119.7 kJ mol^{-1}, respectively (Fig. 7 and Fig. S2 in the supplementary material).[26] These reactions compete unfavorably with the process IS2 → PR7 that occurs directly with loose variational transition states along the path of least energy. The two H atoms in IS2 have distinct roles; when RA involves HCOOD, PR7 becomes OD + HC(O)O. In contrast, when RA involves DCOOH, PR7 becomes OH + DC(O)O.

3. Formation of other minor products

Minor decomposition products of IS8 and IS2 include PR4 (CO_3 + H_2, −243.5 kJ mol^{-1}), formed from IS8 via T8P41 (−120.9 kJ mol^{-1}) and PR5 (CO_2 + H_2O_2,

$-325.1\,kJ\,mol^{-1}$), formed from IS2 via T2P5 ($-76.6\,kJ\,mol^{-1}$). Two additional minor products are also shown in Fig. 7; they are much less important because of the greater energies of the transition states. PR1 ($H_2CO + O_2$, $-190.0\,kJ\,mol^{-1}$) is formed from IS1 ($-94.6\,kJ\,mol^{-1}$) and IS7 ($-160.2\,kJ\,mol^{-1}$) via T1P1 ($21.3\,kJ\,mol^{-1}$) and T7P1 ($79.9\,kJ\,mol^{-1}$), in which the H atom migrates from OH to a neighboring C atom. PR2 (H_2O + *cyc*-CO_2, $-127.2\,kJ\,mol^{-1}$) is produced from the migration of the H atom from CH in IS6 (*trans*-$HOC(O_2)H$) to the neighboring OH group via T6P2 ($55.2\,kJ\,mol^{-1}$). Other minor product channels are shown in Fig. S2 of the supplementary material.[26]

4. Direct H abstraction reactions

The direct H-abstraction might proceed via two channels: attacking the OH group to form HC(O)O + OH (H_O abstraction) or attacking the CH group to form HOCO + OH (H_C abstraction). As shown in Fig. 7(b), both abstraction reactions occur via shallow complexes (Com1 and Com2) and transition states (TS1 and TS2) with relative energies of 9.6 and $-2.1\,kJ\,mol^{-1}$, respectively. The H_O abstraction channel is unimportant because of the large barrier. The H_C abstraction channel with a smaller barrier is more important, but its contribution still competes less successfully with the major channels involving IS2 and IS8 because the energy of the transition state of the former channel is much greater than those of the transition states of the latter. Furthermore, both abstraction reactions have tighter transition-state structures than those in the processes described in Secs. IV D 1–IV D 3.

Yang *et al.* provided experimental and theoretical evidence that, in the reaction of $O(^1D)$ with CHD_3, the complex-forming reaction actually proceeds via a trapped abstraction mechanism, rather than an insertion mechanism as has long been thought.[41] Our MRCI calculations for the direct abstraction reactions did locate similar but much weaker pre-reaction complexes. Because the yields of OH from the abstraction channels are too small to compete with those from the insertion/decomposition channels, we are unable to characterize the importance of this trapped abstraction mechanism with experiments.

E. Calculations of rate coefficients

1. Kinetics of $O(^1D)$ reaction with HCOOH

According to the predicted PES, the energetically favored channels in the reaction of $O(^1D)$ + HCOOH are summarized below:

$$O(^1D) + HCOOH \rightarrow IS8^*(C-H\ \text{insertion}) \rightarrow CO_2 + H_2O, \quad (1)$$

$$\rightarrow OH + HOCO, \quad (2)$$

$$\rightarrow CO_3 + H_2, \quad (3)$$

$$O(^1D) + HCOOH \rightarrow IS1^* \rightarrow IS2^*(O-H\ \text{insertion}) \rightarrow OH + HC(O)O, \quad (4)$$

$$\rightarrow CO_2 + H_2O, \quad (5)$$

in which ISn* denotes an internally activated intermediate and reactions (3) and (5) are minor.

The initial average kinetic energy of $O(^1D)$ that is produced upon photolysis of O_3 at 248 nm was determined to be $36\,kJ\,mol^{-1}$ in the laboratory coordinates.[42] In the center-of-mass coordinates of the collision of $O(^1D)$ with HCOOD or DCOOH, the kinetic energy is estimated to be $26.9\,kJ\,mol^{-1}$. The reactants thus have excess energy $\sim 27\,kJ\,mol^{-1}$. This amount of energy is included in the calculations for fragmentation.

As discussed above, the initial association path via a direct C−H insertion forms an excited IS8 intermediate carrying internal energy as much as $27 + 681 = 708\,kJ\,mol^{-1}$ and produces various products H_2O, OH, and H_2 (reactions (1)–(3)). This process has no well-defined transition state; its potential-energy function for association, computed variationally to cover the C−O separations from 1.4 to 5.0 Å at the CASPT2//CASSCF level, was fitted to a Morse function with $\beta = 2.96\ Å^{-1}$. The internal rotation of the OH group in *cis-cis*-HOC(O)OH (IS8) has a barrier of $39.7\,kJ\,mol^{-1}$. This internal rotation gives rise to a torsional vibrational mode near $197\,cm^{-1}$, which is treated as a hindered rotor.

The excited IS2 intermediate, produced via IS1*, carries internal energy as much as $27 + 341 = 368\,kJ\,mol^{-1}$. For the initial association channel of $O(^1D)$ + HCOOH→ IS1*, we used a Morse potential with $\beta = 2.64\ Å^{-1}$. The rate coefficients were calculated with the unified statistical formulation of Miller,[43] taking into account the multiple reflection corrections above the shallow wells of the pre-reaction complex IS2 on treating T1/2 as the inner TS and the VTS for the pre-complex formation as the outer TS.

The rate coefficients of important product channels via IS8 and IS2 for reactions $O(^1D)$ + HCOOH, HCOOD, and DCOOH are listed in Table II. At $T = 350$ K and $P = 0.1$ Torr, the internally-excited adducts readily undergo H-migration and fragmentation producing various products; these reactions are competitive with the collisional quenching process that depends on pressure. The rate coefficients for the initial association path of $O(^1D)$ + HCOOH → IS8* at 350 and 298 K are predicted to be 9.6 and $9.1 \times 10^{-11}\ cm^3\ molecule^{-1}\ s^{-1}$, respectively. The rate coefficients for $O(^1D)$ + HCOOH → IS2* at 350 and 298 K are predicted to be 7.3 and $7.0 \times 10^{-11}\ cm^3\ molecule^{-1}\ s^{-1}$. As discussed in Sec. IV D, the contributions from the abstraction channels of H atoms on the O−H and C−H moieties of HCOOH to form OH are negligible because of their tighter transition states with energies of 9.6 (TS1) and −2.1 (TS2) $kJ\,mol^{-1}$, respectively, relative to the reactants:

$$O(^1D) + HCOOH \rightarrow Com1(H_O\ \text{abstraction}) \rightarrow OH + HC(O)O, \quad (6)$$

$$O(^1D) + HCOOH \rightarrow Com2(H_C\ \text{abstraction}) \rightarrow OH + HOCO. \quad (7)$$

Rate coefficient $k_7 = 1.5 \times 10^{-11}\ cm^3\,molecule^{-1}\,s^{-1}$ for the H_C-abstraction at 350 K is much greater than that for

TABLE II. Rate coefficients (in cm^3 $molecule^{-1}$ s^{-1}) predicted for important reactions of $O(^1D)$ + HCOOH with excess energy E^* (in kJ mol^{-1}) based on potential-energy surfaces predicted with the CCSD(T)/6-311++G(3df,2p)// B3LYP/6-311++G(3df,2p) method.

	Reaction Products	$T = 298$ K[a] $E^* = 0$	$T = 350$ K[a] $E^* = 0$	$E^* = 12.6$	$E^* = 26.0$
k_1	IS8* → $CO_2 + H_2O$	5.12×10^{-11}	5.32×10^{-11}	4.95×10^{-11}	4.66×10^{-11}
k_2	IS8* → OH + HOCO	4.03×10^{-11}	4.30×10^{-11}	4.63×10^{-11}	5.02×10^{-11}
k_3	IS8* → $CO_3 + H_2$	2.52×10^{-16}	2.92×10^{-16}	4.73×10^{-16}	7.67×10^{-16}
k_4	IS2* → OH + HC(O)O	7.01×10^{-11}	7.30×10^{-11}	7.52×10^{-11}	7.74×10^{-11}
k_5	IS2* → $CO_2 + H_2O$	7.17×10^{-15}	7.86×10^{-15}	1.07×10^{-14}	1.44×10^{-14}
k_6	OH + HC(O)O (H_O-abs)	3.99×10^{-14}	3.86×10^{-14}	...	...
k_7	OH + HOCO (H_C-abs)	1.55×10^{-11}	1.48×10^{-11}	...	...

[a]Rate coefficients are independent of pressure for $P \leq 20$ atm.

the H_O-abstraction, $k_6 = 3.9 \times 10^{-14}$ cm^3 $molecule^{-1}$ s^{-1}, but contributes only ~8% of the total rate coefficient. Other channels have rate coefficients smaller than 4×10^{-14} cm^3 $molecule^{-1}$ s^{-1}. The predicted total rate coefficients for reaction of $O(^1D)$ + HCOOH at 298 K is 1.8×10^{-10} cm^3 $molecule^{-1}$ s^{-1} for pressure less than 20 atm. This result is in accord with the rate coefficient of reaction $O(^1D)$ + CH_3OH reported as 5.1×10^{-10} cm^3 $molecule^{-1}$ s^{-1};[30] this reaction involves three H atoms on the carbon atom and one on the oxygen atom as compared with one H atom on the carbon atom and one on the oxygen atom for the reaction of $O(^1D)$ + HCOOH.

The rate coefficients for the unimolecular decomposition of excited intermediate IS8* at varied energies, presented in Fig. 10, indicate that reactions (1) and (2) that produce CO_2 + H_2O and OH + HOCO, respectively, are competitive, but reaction (3) for the production of CO_3 + H_2 is unimportant in the energy range of interest. According to Fig. 10, reaction (1) dominates up to $E \cong 700$ kJ mol^{-1}; above that, reaction (2) becomes more important. The rate coefficients of these two channels are similar, with <50% variations, for excess energy 0−63 kJ mol^{-1}. The rate coefficients for the unimolecular decomposition of IS2* are shown in Fig. 11; channel IS2* → OH + HC(O)O, reaction (4), is much more important than the channel for formation of CO_2 + H_2O, reaction (5), because of the much larger barrier for the latter. Based on the calculated rate coefficient for the formation of IS8, IS2, and the ratios of unimolecular rate coefficients for each decomposition channel, we derived rate coefficients for each product channel at 350 K and below 20 atm with excess energies 0, 12.6, and 26.0 kJ mol^{-1}, as listed in Table II; the two abstraction channels are also listed for comparison.

2. Formation of OH and OD from $O(^1D)$ + HCOOD

Taking into account of the isotopic effects, we calculated rate coefficients for the unimolecular decomposition of excited intermediates IS8* and IS2* at varied energies in the reaction $O(^1D)$ + HCOOD, as presented in Figs. S4 and S5, respectively, available in the supplementary material.[26] The bimolecular rate coefficients for each product channel of $O(^1D)$ + HCOOD at 350 K and below 20 atm, with excess energies 0, 12.6, and 26.0 kJ mol^{-1}, are listed in Table III; those at 298 K with no excess energy are also listed for comparison.

The following paths are important for $O(^1D)$ + HCOOD:

$$O(^1D) + HCOOD \rightarrow HOC(O)OH\,(IS8^*,\ C-H\ \text{insertion})$$
$$\rightarrow CO_2 + HDO, \quad (8)$$

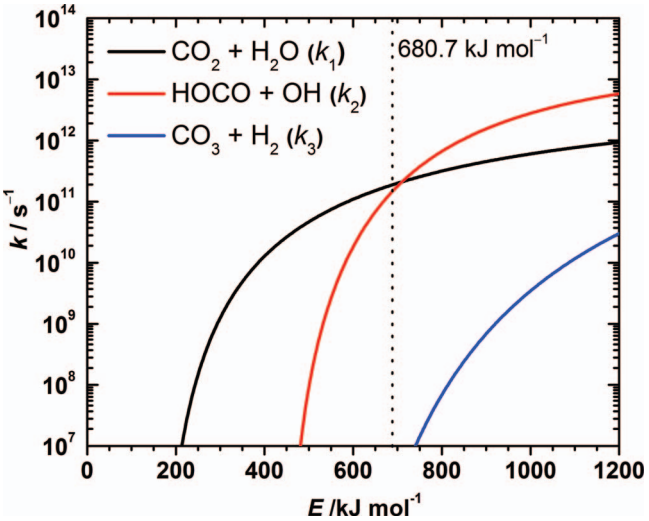

FIG. 10. Predicted rate coefficients k_1-k_3 of the unimolecular decomposition channels of HOC(O)OH (IS8) as a function of energy.

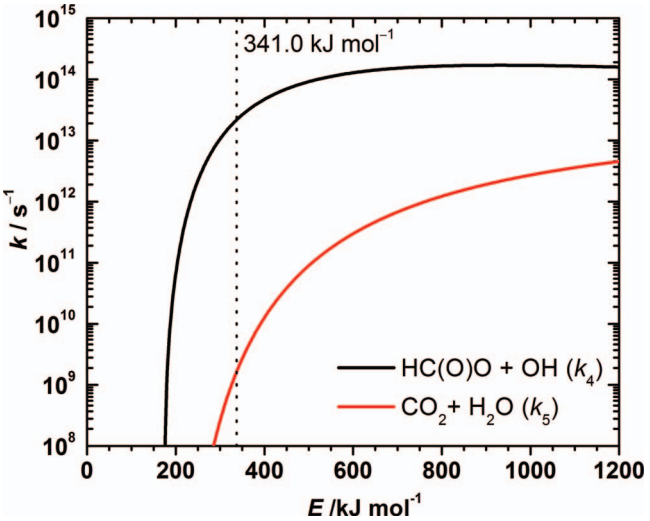

FIG. 11. Predicted rate coefficients k_4 and k_5 of the unimolecular decomposition channels of HC(O)OOH (IS2) as a function of energy.

TABLE III. Rate coefficients (in cm^3 $molecule^{-1}$ s^{-1}) predicted for major channels of production of OH/OD and CO_2 in reactions $O(^1D)$ + HCOOD and DCOOH with excess energy E^* (in kJ mol^{-1}) based on potential-energy surfaces predicted with the CCSD(T)/6-311++G(3df,2p)// B3LYP/6-311++G(3df,2p) method.

	Reaction	$T = 298$ K[a] $E^* = 0$	$T = 350$ K[a] $E^* = 0$	$E^* = 12.6$	$E^* = 26.0$
$O(^1D)$ + HCOOD					
k_8	$IS8^* \rightarrow CO_2 + HDO$	2.18×10^{-11}	2.27×10^{-11}	2.06×10^{-11}	1.89×10^{-11}
k_9	$IS8^* \rightarrow OH + DOCO$	1.56×10^{-11}	1.66×10^{-11}	1.75×10^{-11}	1.87×10^{-11}
k_{10}	$IS8^* \rightarrow OD + HOCO$	1.51×10^{-11}	1.61×10^{-11}	1.69×10^{-11}	1.80×10^{-11}
k_{11}	$IS2^* \rightarrow OD + HC(O)O$	7.02×10^{-11}	7.34×10^{-11}	7.40×10^{-11}	7.63×10^{-11}
k_{12}	$IS2^* \rightarrow CO_2 + HDO$	7.89×10^{-15}	8.74×10^{-15}	1.17×10^{-14}	1.59×10^{-14}
$O(^1D)$ + DCOOH					
k_{13}	$IS8^* \rightarrow CO_2 + HDO$	2.15×10^{-11}	2.22×10^{-11}	2.01×10^{-11}	1.79×10^{-11}
k_{14}	$IS8^* \rightarrow OD + HOCO$	2.20×10^{-11}	2.33×10^{-11}	2.44×10^{-11}	2.53×10^{-11}
k_{15}	$IS8^* \rightarrow OH + DOCO$	2.41×10^{-11}	2.41×10^{-11}	2.53×10^{-11}	2.62×10^{-11}
k_{16}	$IS2^* \rightarrow OH + DC(O)O$	7.02×10^{-11}	7.43×10^{-11}	7.47×10^{-11}	7.71×10^{-11}
k_{17}	$IS2^* \rightarrow CO_2 + HDO$	3.28×10^{-15}	3.11×10^{-15}	4.14×10^{-14}	6.01×10^{-14}

[a]Rate coefficients are independent of pressure for $P \leq 20$ atm.

$$\rightarrow \text{OH} + \text{DOCO (fission of new C}-\text{O bond)}, \quad (9)$$

$$\rightarrow \text{OD} + \text{HOCO (fission of original C}-\text{O bond)}, \quad (10)$$

$$\text{O}(^1\text{D}) + \text{HCOOD} \rightarrow \text{IS1}^*$$

$$\rightarrow \text{HC(O)OOH (IS2}^*, \text{ O}-\text{D insertion)}$$

$$\rightarrow \text{OD} + \text{HC(O)O (fission of O}-\text{O bond)}, \quad (11)$$

$$\rightarrow \text{CO}_2 + \text{HDO}. \quad (12)$$

The predicted results indicate one production channel for OH (rate coefficient k_9) and two for OD (k_{10} and k_{11}) in $O(^1D)$ + HCOOD. At 350 K with the center-of-mass kinetic energy of 26 kJ mol^{-1}, the rate coefficients are $k_9 = 1.9 \times 10^{-11}$ cm^3 $molecule^{-1}$ s^{-1} for the production of OH and $k_{10} = 1.8 \times 10^{-11}$ and $k_{11} = 7.6 \times 10^{-11}$ cm^3 $molecule^{-1}$ s^{-1} for the production of OD. Thus, for $O(^1D)$ + HCOOD, the ratio of $k_{OH}/k_{OD} = (k_9)/(k_{10} + k_{11})$ is 0.20, which is in good agreement with the experimental value of [OH]/[OD] = 0.16 ± 0.05. The predicted ratios k_{OH}/k_{OD} as a function of excess energy are presented in Fig. 12; these values are insensitive to the excess energy carried by the $O(^1D)$ atom. For example, at no excess energy the predicted ratio of k_{OH}/k_{OD} is 0.185. Ratio k_{OH}/k_{OD} is independent of pressure below 20 atm because of the large energy content of the adducts, similar to the case of $O(^1D) + CH_3OH$.[7]

In the $O(^1D)$ + HCOOD reaction, the rotational distribution of the product OD is bimodal, whereas that of OH is of Boltzmann-like. The bimodal rotational distribution of OD is consistent with the model that predicts OD be produced via two channels, reactions (10) and (11). The former resulted from the insertion of $O(^1D)$ into the C−H bond to form IS8, followed by fission of the "original" OD; the latter resulted from the insertion of $O(^1D)$ into the O−D bond to form IS2, followed by fission of OD. We expect that the OD produced from the latter channel via IS2 has greater rotational excitation because the torque angle for OD fission in IS2 is much greater than that of IS8 (Fig. 8); a similar situation was observed for $O(^1D) + CH_3OD$.[7] For the channels from IS8, HOC(O)OD, products OD + HOCO and OH + DOCO have more excess energy (227.6 kJ mol^{-1}) than that of products OD + HC(O)O from IS2 (168.2 kJ mol^{-1}); product OD + HOCO resulted from fission of the original C−O bond, whereas OH + DOCO was produced from fission of the newly formed C−O bond. Our observation of a similar vibrational energy for OH than for the low-J component of OD in the reaction of $O(^1D)$ + HCOOD might indicate that IVR was nearly complete before the bond fission because OD was indirectly activated through IVR from the locally excited intermediate HOC(O)OD produced from the C−H insertion. The Boltzmann-like distribution of OH is consistent with a single channel for the production of OH from reaction (9).

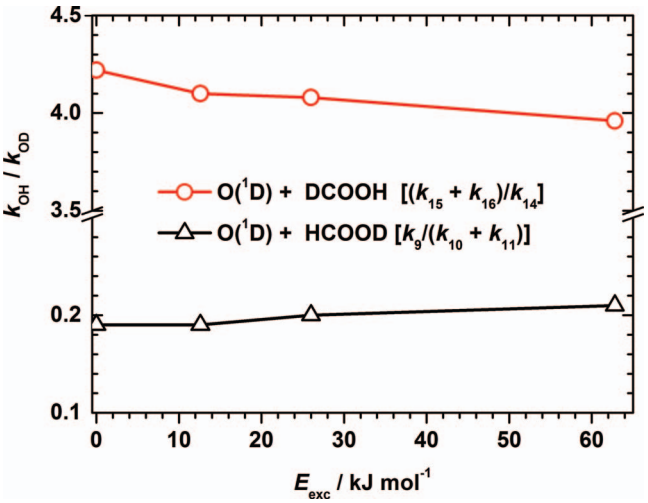

FIG. 12. Predicted ratios of k_{OH}/k_{OD} for reactions of $O(^1D)$ + HCOOD (symbol Δ) and $O(^1D)$ + DCOOH (symbol o) as a function of excess energy E_{exc} relative to the reactants at 350 K.

3. Formation of OH and OD from $O(^1D)$ + DCOOH

The rate coefficients for the unimolecular decomposition of excited intermediates IS8* and IS2* at varied energies in the reaction $O(^1D)$ + DCOOH are presented in Figs. S6 and S7 of the supplementary material, respectively.[26] The bimolecular rate coefficients for each product channel of $O(^1D)$ + DCOOH at 350 K and below 20 atm, with excess energies 0, 12.6, and 26.0 kJ mol^{-1}, are listed in Table III; those at 298 K with no excess energy are also listed for comparison.

The pathways for $O(^1D)$ + DCOOH can be summarized as follows:

$$O(^1D) + DCOOH \rightarrow DOC(O)OH\,(IS8^*,\ C-D\ \text{insertion})$$
$$\rightarrow CO_2 + HDO, \quad (13)$$
$$\rightarrow OD + HOCO\,(\text{fission of new C}-\text{O bond}), \quad (14)$$
$$\rightarrow OH + DOCO\,(\text{fission of original C}-\text{O bond}), \quad (15)$$
$$O(^1D) + DCOOH \rightarrow IS1^*$$
$$\rightarrow DC(O)OOH\,(IS2^*,\ O-H\ \text{insertion})$$
$$\rightarrow OH + DC(O)O\,(\text{fission of O}-\text{O bond}), \quad (16)$$
$$\rightarrow CO_2 + HDO. \quad (17)$$

At 350 K with the center-of-mass kinetic energy of 26 kJ mol^{-1}, the rate coefficients are $k_{15} = 2.6 \times 10^{-11}$ and $k_{16} = 7.7 \times 10^{-11}$ cm^3 molecule^{-1} s^{-1} for the production of OH and $k_{14} = 2.5 \times 10^{-11}$ cm^3 molecule^{-1} s^{-1} for the production of OD. For reaction $O(^1D)$ + DCOOH, the ratio of $k_{OH}/k_{OD} = (k_{15} + k_{16})/(k_{14})$ is thus 4.08. Predicted ratios k_{OH}/k_{OD} as a function of kinetic energy are presented in Fig. 12; they are insensitive to the excess energy carried by the $O(^1D)$ atom. For example, at no kinetic energy the predicted ratio of k_{OH}/k_{OD} is 4.2. The experimental value of [OH]/[OD] is unavailable because the OD signal was too weak to yield reliable data; [OD] is much smaller than [OH], and the Einstein coefficients of OD are smaller than those of OH by more than a factor of four.

The rotational distribution of OH was found to be bimodal, consistent with the model that OH is produced via two channels, reactions (15) and (16). The former resulted from insertion of $O(^1D)$ into the C−D bond to form IS8, followed by fission of the "original" OH, whereas the latter resulted from insertion of $O(^1D)$ into the O−H bond to form IS2, followed by fission of OH. We expect that OH produced from the latter channel via IS2 has greater rotational excitation because the torque angle for OD fission in IS2 is much greater than that of IS8 (Fig. 8); a similar situation was observed for $O(^1D) + CH_3OD$.[7]

4. Formation of CO_2

The major channel for formation of CO_2 is predicted to be from IS8 (C−H insertion) via T8P6 at −500.5 kJ mol^{-1}. The formation of CO_2 is unaffected by the deuterium isotopic substitution; reaction products (8) and (13) are hence identical. Products from reactions (12) and (17) via IS2 (O−H or O−D insertion) and T2P6 at −119.7 kJ mol^{-1} are negligible because of the large barrier, but the product of reaction (11) or (16), HC(O)O or DC(O)O, might undergo a secondary decomposition to form CO_2 because the barrier is less than 1.3 kJ mol^{-1}. Secondary decomposition of HOCO or DOCO, produced in reaction (10) and (15), is less likely because of a large barrier of 109.2 kJ mol^{-1} with TP8P11 lying at −118.4 kJ mol^{-1}. Hence, the decomposition of the C−H insertion intermediate IS8 and the secondary decomposition of HC(O)O that is produced from the decomposition of O−H insertion intermediate IS2 are two major channels for the formation of CO_2. If we assume that the yield of secondary decomposition of HC(O)O to H + CO_2 is large, CO_2 produced from this channel is expected to be dominant.

Assuming that the translational energy is mainly contributed by the downhill slope from the transition state, we estimate the translational energy of H + CO_2 to be approximately the energy difference between TP7P11 and PR11, 64 kJ mol^{-1}. Considering the exothermicity for the formation of PR11 (OH + H + CO_2), 231 kJ mol^{-1}, and the estimated translational energy of 64 kJ mol^{-1}, our observed internal energy of OH (OD), 46 (47) kJ mol^{-1} for the high-J component observed in $O(^1D)$ + DCOOH/HCOOD, implies that the internal energy of CO_2 might be as large as ∼120 kJ mol^{-1}, consistent with the observed low-energy component of CO_2 with $E^* = 8000$ cm^{-1} (96 kJ mol^{-1}). The predicted C−O bond of length ∼1.176 Å in TP7P11 is slightly greater than the bond length of 1.160 Å for CO_2, also indicating a moderate vibrational excitation of the CO_2 product from this channel. The relative population of this component is ∼53%.

For the minor channel from the decomposition of IS8, taking the exothermicity for formation of PR6 ($H_2O + CO_2$) to be 712 kJ mol^{-1}, and assuming that the translational energy is contributed mainly from the energy difference of 211 kJ mol^{-1} between T8P6 and PR6, ∼501 kJ mol^{-1} energy is partitioned among the internal energies of CO_2 and H_2O. The quantum-chemical calculations predicted structure of the transition state T8P6 with a H_2O moiety with a bond angle of 119.8° and bond lengths of OH as 1.247 and 0.965 Å, and a CO_2 moiety with bond angle 145.8° and bond lengths of CO as 1.257 and 1.167Å, respectively (Fig. 9). Considering the equilibrium bond lengths of 0.958 Å for H_2O and 1.160 Å for CO_2 and the linear structure of CO_2, we expect that CO_2 be more vibrationally excited than H_2O. The observed high-energy component of CO_2 with $E^* = 26\,500$ cm^{-1} (317 kJ mol^{-1}) is consistent with this model. The relative population of this component is ∼47%.

V. CONCLUSION

On monitoring the IR emission of products OH and OD with a step-scan Fourier-transform infrared spectrometer, we investigated the reactions $O(^1D)$ + HCOOD/DCOOH. In the reaction $O(^1D)$ + HCOOD, product OD showed bimodal rotational distributions with nascent average rotational energies 6 ± 2 and 25 ± 6 kJ mol^{-1} and vibrational energies

38 ± 4 and 22 ± 3 kJ mol^{-1}, respectively, whereas product OH showed a Boltzmann-like rotational distribution with nascent average rotational energies 8 ± 2 kJ mol^{-1} and vibrational energies 40 ± 4 kJ mol^{-1}. The product ratio [OH]/[OD] was estimated to be 0.16 ± 0.05. For reaction O(^{1}D) + DCOOH, product OH showed a bimodal rotational distribution with nascent average rotational energies 7 ± 2 and 26 ± 4 kJ mol^{-1} and vibrational energies 38 ± 4 and 20 ± 3 kJ mol^{-1}, respectively. Lines of OD were too weak to provide reliable information.

In both reactions, similar unresolved internally excited ν_3 emission of CO_2 was observed. The emission band was deconvoluted to two components that were simulated according to a statistical partition of excess energy; the low-energy component with E^* = 96 kJ mol^{-1} is dominant with ~53% population, whereas the high-energy component with E^* = 317 kJ mol^{-1} has ~47% population.

The experimental observations are explicable according to a mechanism of O(^{1}D) + HCOOH that involves two insertion intermediates, HOC(O)OH (IS8, from C−H insertion) and HC(O)OOH (IS2, from O−H insertion), and three major decomposition channels, reactions (1) and (2) from IS8 to produce CO_2 + H_2O and OH + HOCO, respectively, and reaction (4) from IS2 to produce OH + HC(O)O. The internally excited HC(O)O further decomposed to H + CO_2. In reaction (2), upon insertion of O(^{1}D) into the C−H bond to form HOC(O)OH, subsequent fission of the newly formed C−O bond and fission of the "original" C−O bond in HOC(O)OH produced vibrationally excited OH with similar vibrational excitation, indicating nearly completed IVR. Insertion of O(^{1}D) into the O−H bond to form HC(O)OOH followed by fission of the O−O bond, reaction (4), produced OH with greater rotational excitation, likely due to a large torque angle during dissociation. In the reaction O(^{1}D) + HCOOD, the observed ratio of [OH]/[OD] = 0.16 ± 0.05 is near a value of 0.20 predicted with theory. The two abstraction channels are unimportant.

For the production of CO_2, the high-energy component corresponded to direct decomposition of the C−H insertion intermediate HOC(O)OH (IS8), whereas the low-energy component was due to secondary decomposition of internally excited HC(O)O that was produced from decomposition of the O−H insertion intermediate HC(O)OOH (IS2).

Even though the observed [OH]/[OD] indicates a significant preference of the formation of OH from the hydroxyl moiety over the CH moiety of HCOOH, the theoretical predictions indicate that the rate coefficients for O(^{1}D) to attack the CH moiety and the OH moiety of HCOOH are similar, with the former more favored in O(^{1}D) + HCOOH by ~30% and the latter more favored in O(^{1}D) + HCOOD or DCOOH by ~40%. The reason for production of more OH from the hydroxyl site is partly that, upon insertion of O(^{1}D) into the C−H bond to form HOC(O)OH, subsequent dissociation occurred for both the newly formed OH and the original OH group, and partly that this C−H insertion intermediate HOC(O)OH also decomposed to form CO_2 and H_2O, whereas the decomposition of O−H insertion intermediate HC(O)OOH produced mainly OH + HC(O)O.

ACKNOWLEDGMENTS

Ministry of Science and Technology of Taiwan (Grant No. MOST103-2745-M-009-001-ASP) and the Ministry of Education, Taiwan ("Aim for the Top University Plan" of National Chiao Tung University) supported this work. The National Center for High-performance Computing provided computer time and facilities. M.C.L. acknowledges the support from the NSC for the distinguished visiting professorship at National Chiao Tung University in Hsinchu, Taiwan.

[1] J. R. Wiesenfeld, Acc. Chem. Res. **15**, 110 (1982).
[2] R. F. Heidner III, D. Husain, and J. R. Wiesenfeld, J. Chem. Soc., Faraday Trans. 2 **69**, 927 (1973).
[3] C. R. Park and J. R. Wiesenfeld, J. Chem. Phys. **95**, 8166 (1991).
[4] A. C. Luntz, J. Chem. Phys. **73**, 1143 (1980).
[5] S. Wada and K. Obi, J. Phys. Chem. A **102**, 3481 (1998).
[6] X. Yan, Phys. Chem. Chem. Phys. **8**, 205 (2006).
[7] C.-K. Huang, Z.-F. Xu, M. Nakajima, H. M. T. Nguyen, M. C. Lin, S. Tsuchiya, and Y.-P. Lee, J. Chem. Phys. **137**, 164307 (2012).
[8] H. G. Yu, H. T. Muckerman, and H. S. Francisco, J. Phys. Chem. A **109**, 5230 (2005).
[9] L. Khriachtchev, A. Domanskaya, K. Marushkevich, M. Räsänen, B. Grigorenko, A. Ermilov, N. Andrijchenko, and A. Nemukhin, J. Phys. Chem. A **113**, 8143 (2009).
[10] P.-S. Yeh, G.-H. Leu, Y.-P. Lee, and I-C. Chen, J. Chem. Phys. **103**, 4879 (1995).
[11] S.-R. Lin and Y.-P. Lee, J. Chem. Phys. **111**, 9233 (1999).
[12] C.-Y. Wu, C.-Y. Chung, Y.-C. Lee, and Y.-P. Lee, J. Chem. Phys. **117**, 9785 (2002).
[13] S.-K. Yang, S.-Y. Liu, H.-F. Chen, and Y.-P. Lee, J. Chem. Phys. **123**, 224304 (2005).
[14] Y. Matsumi and M. Kawasaki, Chem. Rev. **103**, 4767 (2003).
[15] L. T. Molina and M. J. Molina, J. Geophys. Res. **91**, 14501, doi: 10.1029/JD091iD13p14501 (1986).
[16] J. Chao and B. J. Zwolinski, J. Phys. Chem. Data **7**, 363 (1978).
[17] A. D. Becke, J. Chem. Phys. **98**, 5648 (1993); C. Lee, W. Yang, and R. G. Parr, Phys. Rev. B **37**, 785 (1988).
[18] J. A. Pople, M. Head-Gordon, and K. Raghavachari, J. Chem. Phys. **87**, 5968 (1987).
[19] H.-J. Werner and P. J. Knowles, J. Chem. Phys. **82**, 5053 (1985); P. J. Knowles and H.-J. Werner, Chem. Phys. Lett. **115**, 259 (1985).
[20] H.-J. Werner, P. J. Knowles, G. Knizia, F. R. Manby, M. Schütz *et al.*, MOLPRO is a package of *ab initio* programs MOLPRO, version 2009.1, a package of *ab initio* programs, 2009, see http://www.molpro.net.
[21] M. J. Frisch, G. W. Trucks, H. B. Schlegel *et al.*, GAUSSIAN 09, Revision E.01, Gaussian, Inc., Wallingford, CT, 2004.
[22] S. J. Klippenstein, A. F. Wagner, R. C. Dunbar, D. M. Wardlaw, and S. H. Robertson, VARIFLEX: Version 1.00, 1999.
[23] S. J. Klippenstein, J. Chem. Phys. **96**, 2155 (1992).
[24] S. J. Klippenstein and M. A. Marcus, J. Chem. Phys. **87**, 3410 (1987).
[25] C. Eckart, Phys. Rev. **35**, 1303 (1930).
[26] See supplementary material at http://dx.doi.org/10.1063/1.4897418 for comparison of tunneling corrections, plot of rotational temperature T_R of OH from O(^{1}D) + DCOOH as a function of time, a complete potential-energy scheme and additional optimized geometries of transition states, and predicted rate coefficients k_8−k_{17} as a function of energy.
[27] J. G. Chang, H. T. Chen, S. Xu, and M. C. Lin, J. Phys. Chem. A **111**, 6789 (2007).
[28] F. M. Mourit and F. H. A. Rummens, Can. J. Chem. **55**, 3007 (1977).
[29] H. Hippler, J. Troe, and H. J. Wendenlken, J. Chem. Phys. **78**, 6709 (1983).
[30] Y. Matsumi, Y. Inagaki, and M. Kawasaki, J. Phys. Chem. **98**, 3777 (1994).
[31] M. C. Abrams, S. P. Davis, M. L. P. Rao, and R. Engelman, Jr., J. Mol. Spectrosc. **165**, 57 (1994).
[32] H.-F. Chen, H.-C. Chiang, H. Matsui, S. Tsuchiya, and Y.-P. Lee, J. Phys. Chem. A **113**, 3431 (2009).
[33] M. Pettersson, J. Lundell, L. Khriachtchev, and M. Räsänen, J. Am. Chem. Soc. **119**, 11715 (1997).
[34] F. Holtzberg, B. Post, and I. Fankuchen, Acta Crystallogr. **6**, 127 (1953).
[35] H. Yamazaki and R. J. Cvetanovic, J. Chern. Phys. **41**, 3703 (1964).

[36]W. B. Demore and O. F. Raper, J. Chern. Phys. **46**, 2500 (1967).
[37]P. P. Kumar, A. G. Kalinichev, and R. J. Kirkpatrick, J. Chem. Phys. **126**, 204315 (2007).
[38]T. Mori, K. Suma, Y. Sumiyoshi, and Y. Endo, J. Chem. Phys. **134**, 044319 (2011).
[39]T. Mori, K. Suma, Y. Sumiyoshi, and Y. Endo, J. Chem. Phys. **130**, 204308 (2009).
[40]H. G. Yu, J. T. Mukerman, and T. J. Sears, Chem. Phys. Lett. **349**, 547 (2001).
[41]J. Yang, K. Shao, D. Zhang, Q. Shuai, B. Fu, D. H. Zhang, and X. Yang, J. Phys. Chem. Lett. **5**, 3106 (2014).
[42]M.-A. Thelen, T. Gejo, J. A. Harrison, and J. R. Huber, J. Chem. Phys. **103**, 7946 (1995).
[43]W. H. Miller, J. Chem. Phys. **65**, 2216 (1976).